V European Conference on Computational Fluid Dynamics
ECCOMAS CFD 2010
J. C. F. Pereira and A. Sequeira (Eds)
Lisbon, Portugal,14-17 June 2010

COMPUTATIONAL HEMODYNAMICS OF INTRACRANIAL ANEURYSMS: MODELLING AND GEOMETRICAL SENSITIVITY

A. Gambaruto*, J. Janela†, A. Moura* and A. Sequeira*

*CEMAT, Center for Mathematics and its Applications, Department of Mathematics, IST,
Instituto Superior Técnico, Tecnical University of Lisbon
Av. Rovisco Pais, 1, 1049-001, Lisboa, Portugal
e-mail: {agambar, alexandra.moura, adelia.sequeira}@math.ist.utl.pt

†CEMAT and Department of Mathematics, ISEG, School of Economics and Management,
Technical University of Lisbon
Rua do Quelas, 6, 1200-781, Lisboa, Portugal
e-mail: {jjanela}@iseg.utl.pt

Key words: Blood flow modeling, medical image reconstruction, non-Newtonian fluids.

Abstract. *Local hemodynamics has long been recognized to play a significant role in the location and development of vascular diseases. Although in many studies found in literature blood is modelled as a Newtonian fluid, it exhibits rheological characteristics such as shear-thinning viscosity, viscoelasticity and yield stress and, in some physiological flow conditions, more complex non-Newtonian models should be used. The choice of the mathematical model describing blood flow can considerably affect the amount of computational work involved in the simulations, as well as the type of effects that can be predicted or reproduced at the numerical level. In particular, cerebral aneurysms exhibit a range of shear stresses, indicating that non-Newtonian effects are very important.*

In this study Newtonian and generalized Newtonian mathematical models are compared in an anatomically realistic geometry of cerebral aneurysms, reconstructed from rotational CTA. Different levels of smoothing are also applied to the reconstructed virtual model. The impact of the mathematical model choice, as well as the smoothing intensity, are used to gauge uncertainty in the numerical simulations. The impact of uncertainty on the computed solution is assessed with respect to clinically relevant fluid mechanics parameters, such as wall shear stress and derived measures.

1 INTRODUCTION

An increasing demand from the medical community for scientifically rigorous and quantitative investigations of vascular diseases has recently given a major impulse to the development of mathematical models and numerical tools for the computer simulations of the human cardiovascular and cerebrovascular systems, in both healthy and pathological states. The cardiovascular system is not static degrading over time, but rather is capable of growth and remodeling in response to changes in mechanical and biochemical stimuli [6, 9]. The initiation and progression of a number of threatening diseases, like intracranial aneurysms (ICA) are believed to be intimately tied to the inability of the vasculature to respond satisfactorily to such complex changes.

ICA appear commonly at the apices of bifurcations and outer walls of curved arterial segments. It has been postulated that ICA formation, growth and rupture are associated with local hemodynamics as well as lumen structural mechanics. Commonly, parameters associated with diseases in the cerebrovascular system are the located at or near the lumen wall, including wall shear stress (WSS), and indicators of disturbed flow, both of which are related to the local and large-scale conduit morphology.

The role of blood flow physiological parameters regulating aneurysm morphology and natural history is poorly understood [7]. The mechanical response of blood largely depends on the state of its red blood cells (RBCs), since these are the dominant constituents. Under differnt flow conditions RBCs can range from three dimensional structures to relatively uniformly dispersed individual cells. Throughout most of the arterial system of healthy individuals, the RBCs are dispersed and it is considered sufficient to model blood as an inelastic, constant viscosity fluid (Newtonian) [8]. However, in some disease states the vascular geometry is locally altered and induces relatively stable regions of slow recirculation (e.g. in ICA or downstream of a stenosis). In such cases, non-Newtonian behavior may become important and constitutive models capturing shear-thinning viscosity, viscoelasticity, thixotropy or yield-stress could be necessary [12, 13, 1, 2].

Moreover, since blood flow dynamics strongly depends on conduit geometry, it is necessary to use anatomically realistic geometries. Medical data acquisition has greatly progressed with recent development of high resolution imaging that is tendencially non-invasive, providing *in vivo* clinical data that can be readily used to perform both experimental and numerical tests.

Despite the feasibility and capability of performing detailed and sophisticated numerical simulations, the reproducibility of the clinical data is fraught with modeling uncertainty stemming principally from both the errors associated with using *in vivo* data that cannot be benchmarked, and also from mathematical modeling of both the blood, vessel walls and biochemical effects and responses that all play role in cardiovascular diseases.

The present work is devoted to uncertainty in the form of both mathematical modeling for the rehological behaiour of blood and in the reconstruction of an anatomically realistic geometry of a cerebral aneurysm obtained from *in vivo* rotational CTA scan.

2 MEDICAL IMAGE RECONSTRUCTION

The medical images used in this study were obtained *in vivo* from rotational CTA, with resulting voxel resolution of 0.4122 mm on a 512^3 grid. The reconstruction of the virtual 3D geometry for numerical simulations consists in image segmentation, surface extraction, surface smoothing and finally arificial flow boundary creation. The initial surface triangulation is obtained using a constant threshold value for segmenting the image data, and a marching tetrahedra algorithm for extracting the 3D surface. The resulting virtual model of the vasculature is then prepared for the numerical simulations by identifying the regions of interest and removing secondary branches.

Figure 1 shows a portion of the initial cerebral arterial geometry, with some secondary branches and a saccular aneurysm, as well as the region of interest that includes the aneurysm and is used in the numerical simulations.

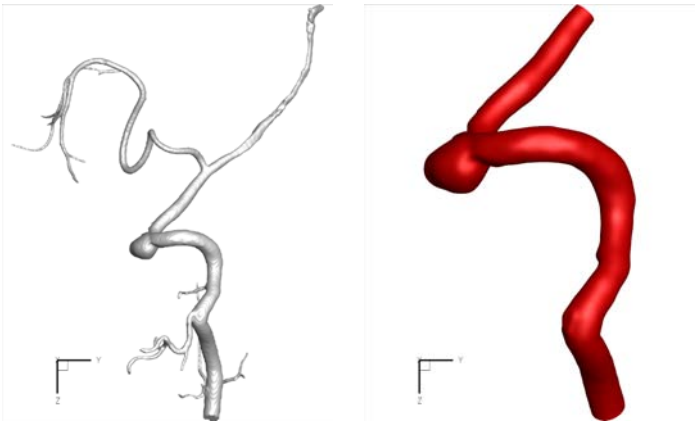

Figure 1: Cerebral arterial system showing a saccular aneurysm located on the outer bend (left). The region of interest for numerical simulations, including the main vessel and the aneurysm (right).

Due to medical imaging noise and limited resolution, the surface definition is not anatomically representative and requires smoothing. This is performed using the bi - Laplacian method, for details see [4] and references therein. It is apparent that there is a degree of uncertainty with respect to the model definition that stems from using *in vivo* data. This is due to the fact that different segmentation and reconstruction procedures will lead to virtual geometry variations, and thus to different numerical solutions of the flow field. Here we focus the study of image reconstruction uncertainty by considering two levels of smoothing, with 300 and 20,000 iterations of the bi-Laplacian method, that corresponds to light and intense smoothing, respectively. For the rest of the paper, the two virtual model definitions are referred to as geometries G_s (lightly smoothed) and G_S (intensely smoothed). These geometry models, with the two different smoothing levels, are shown in Figure 2.

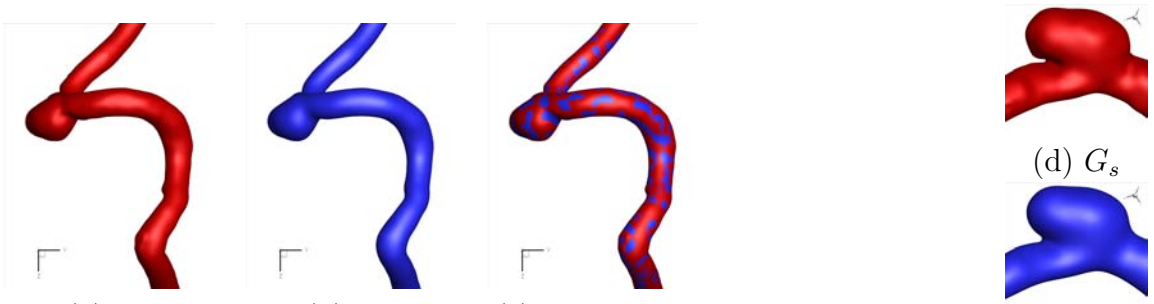

(a) G_s (b) G_S (c) G_s and G_S (d) G_s (e) G_S

Figure 2: (a) Lightly smoothed and (b) intensely smoothed portions of the geometry that are used for the numerical simulations. (c) Overlap of both models and detail in (d), (e).

Clearly, other approaches of inferring uncertainty in the geometry can be sought, using different segmentation and reconstruction methods, as well as different levels of smoothing. Furthermore, different portions of the arterial system to include, for instance, the side branches, or a larger portion for the region of interest also should be considered as geometrical modeling uncertainty. Nevertheless, the study presented here, using the light and intensely smoothed model definitions, as a means of introducing small geometric perturbations, is a good compromise to the level of detail that a rigorous uncertainty analysis would require. It provides a preliminary indicative measure of the effect that geometric variability has on the resulting flow solution.

3 MATHEMATICAL RHEOLOGICAL MODELS

In this work, blood is modeled as an incompressible and isothermal fluid. The governing equations, corresponding to the conservation of mass and linear momentum, can be written as

$$\nabla \cdot \mathbf{u} = 0 \tag{1}$$

$$\rho \left(\frac{\partial \mathbf{u}}{\partial t} + \mathbf{u} \cdot \nabla \mathbf{u} \right) = -\nabla p + \nabla \cdot \boldsymbol{\tau} \tag{2}$$

where ρ is the constant fluid density, $\mathbf{u}$ and p are the fluid velocity and pressure, and $\boldsymbol{\tau}$ is the deviatoric or extra stress tensor. The rheological properties of blood are modeled through the specification of a constitutive relation for $\boldsymbol{\tau}$. In this study, the only non-Newtonian effect that is taken into account is the shear-thinning viscosity. In this case, the extra stress is computed explicitly from the strain rate tensor through the relation

$$\boldsymbol{\tau} = \mu(\dot{\gamma})(\nabla \mathbf{u} + \nabla \mathbf{u}^T). \tag{3}$$

Here, μ is the shear dependent viscosity and $\dot{\gamma}$, the shear rate, is a scalar measure of the strain rate tensor, given by

$$\dot{\gamma} = \sqrt{\frac{1}{2}(\nabla \mathbf{u} + \nabla \mathbf{u}^T) : (\nabla \mathbf{u} + \nabla \mathbf{u}^T)}, \tag{4}$$

The viscosity function, $\mu(\dot{\gamma})$, is fixed *a priori* by fitting experimental viscosity data and can be written in the general form

$$\mu(\dot{\gamma}) = \mu_\infty + (\mu_0 - \mu_\infty) F(\dot{\gamma})$$

, where μ_0 and μ_∞ are the asymptotic viscosities at zero and infinite shear rate, respectively, and $F(\dot{\gamma})$ is a continuous and monotonic function such that

$$\lim_{\dot{\gamma}\to 0} F(\dot{\gamma}) = 0, \qquad \lim_{\dot{\gamma}\to \infty} F(\dot{\gamma}) = 1.$$

Viscosity model

The correct specification of the viscosity model is crucial to capture the correct rheological behavior of blood. In the present work we use viscosity data obtained by Prof. M.V. Kameneva (Univ. Pittsburgh) for normal human blood at 23^oC, for an hematocrit of 40%. Using the estimates found in [10], we converted the data, obtaining realistic viscosity values at 37^o C) (body temperature). The model parameters shown in Table 1 were computed using a non-linear least squares fitting of the viscosity data. More specifically, for each viscosity model of the form $\mu(\dot{\gamma}; \Lambda)$ shown in Table 1, we computed the parameter vector $\Lambda = (\lambda_1, \cdots \lambda_n)$ solution of the minimization problem

$$\Lambda = \underset{\Lambda \in K}{\operatorname{argmin}} \sum_{i=1}^{n} (\mu(\dot{\gamma}_i; \Lambda) - \mu_i)^2,$$

where $K \subset \mathbf{R}^n$ is the set of admissible parameters and μ_i are the measured values of viscosity, for each $\dot{\gamma}_i$. In the numerical optimization procedure, we start by performing an unconstrained optimization, and add the restrictions incrementally (KKT), until all parameters are within physiological ranges.

The most striking fact that can be easily observed in Figure 3 is that the zero shear rate viscosity μ_0 can change considerably, depending on the viscosity model. In that figure we can observe that, although the Carreau and Cross models fit very well the experimental data, they present quite different values regarding the zero shear viscosity. This is related to the lack of viscosity data for very low shear rates which, in the present study, start at a minimum of 0.06 s $^{-1}$. In commonly used parameter sets for blood viscosity models, like the one proposed in [5], the asymptotic viscosities μ_0 and μ_∞ are fixed *a priori* and only the remaining parameters are considered in the numerical fitting. Although this technique removes the heterogeneity in the computed μ_0, in absence of experimental data for very low shear rates there is no valid reason to fix the asymptotic viscosities.

Model	Viscosity Model	Model constants for blood
Carreau	$F(\dot{\gamma}) = (1 + (\lambda\dot{\gamma})^2)^{(n-1)/2}$	$\mu_0 = 0.456, \mu_\infty = 0.032$ $\lambda = 10.03s, n = 0.344$
Cross	$F(\dot{\gamma}) = (1 + (\lambda\dot{\gamma})^m)^{-1}$	$\mu_0 = 0.618, \mu_\infty = 0.034$ $\lambda = 7.683s, m = 0.810$
Yeleswarapu	$F(\dot{\gamma}) = \dfrac{1 + \log(1 + \lambda\dot{\gamma})}{1 + \lambda\dot{\gamma}}$	$\mu_0 = 1.10, \mu_\infty = 0.035$ $\lambda = 45.23s$
Oldroyd	$\mu(\dot{\gamma}) = \mu_0 \dfrac{1 + (\lambda_1\dot{\gamma})^2}{1 + (\lambda_2\dot{\gamma})^2}$	$\mu_0 = 0.426, \mu_\infty = \mu_0\lambda_1^2\lambda_2^{-2}$ $\lambda_1 = 1.09s, \lambda_2 = 3.349s$

Table 1: Selected generalized Newtonian models for blood viscosity with the corresponding material constants. Constants were obtained by nonlinear least squares fit from viscosity data with $Ht = 40\%$ and $T = 37^{\circ}$ C.

In this study the Carreau viscosity model was adopted, with the set of parameters shown in Table 1. The reference constant viscosity considered for the Newtonian vs. non-Newtonian comparisons was $\mu = 0.04$ Poi, corresponding to the average experimental viscosity in the range $\dot{\gamma} \in [6, 1000s]$ s $^{-1}$. Another possible criteria to choose the Newtonian viscosity is to compute the viscosity value that would yield the same volume flow rate in an infinite cylinder of comparable radius. This criteria would give a reference value of $\mu = 0.0345$ Poi. Other criteria and motivation can be sought, however it is important to note that the choice of optimal approxiamtion of constant viscosity dependent on the simulation to be performed, and cannot be estimated a priory, yielding an ulterior modelling uncertainty.

Flow parameters

The fluid equations given by (1) must be endowed with initial and boundary conditions, corresponding to each particular physical problem. In the simulations presented in section 4, the vessel is assumed to be rigid and no-slip conditions are imposed. The fluid starts from rest and is ramped up to a steady state, with a parabolic velocity profile at the inflow section, to correspond to a steady state profile in a straight pipe. The velocity ramp is of the form:

$$\boldsymbol{v}_{in}^{ramp}(x, y, z; t) = \begin{cases} \dfrac{t \cdot \boldsymbol{v}_{in}(x, y, z; t)}{t_{ramp}}, & 0 \leq t < t_{ramp} \\ \\ \boldsymbol{v}_{in}(x, y, x; t), & t \geq t_{ramp} \end{cases}$$

The inlet velocity profile, for $t \geq t_{ramp}$, amounts to a volume flow rate of $Q = 4cm^3s^{-1}$,

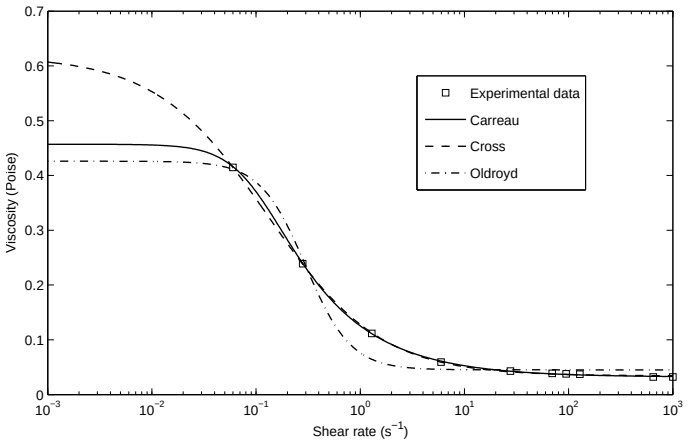

Figure 3: Apparent viscosity as a function of shear rate for whole blood at Ht= 40 %, T = 37^o, obtained using a Contraves LS30 for low shear rates ($\dot{\gamma} \leq 128s^{-1}$) and a CMSM ($\dot{\gamma} \geq 300s^{-1}$).

in agreement with [11]. At the outflow section a no-traction condition is imposed. With these conditions the Reynolds number is $Re = 250$, in the Newtonian case, for a mean radius of 0.25 cm.

Steady state criterion was chosen as a starting point to identify the level of uncertainty in the numerical simulations, that while simplistic can resonably correspond to time averaged unsteady simulations.

Relevant hemodynamic indicators

The importance of using mathematical models to obtain numerical simulations of blood flow in arteries is to obtain highly resolved hemodynamic parameters that are postulated to be linked to diseases, such as atheroma and aneurysms, while noting that other non-mechanical factors of biochemistry play significant roles. The correlators between hemodynamics and disease most commonly sought are the mechanical parameters on and near the wall, such as WSS and derived measures.

The WSS is the tangential stress that the fluid exherts on the wall, hence the tangential component of the stress tensor, which is given by $\boldsymbol{\sigma} = p\mathbf{I} - \boldsymbol{\tau}$, on the wall:

$$WSS = \boldsymbol{\sigma}_\mathbf{n} - (\boldsymbol{\sigma}_\mathbf{n} \cdot \mathbf{n})\mathbf{n} = \boldsymbol{\tau}_\mathbf{n} - (\boldsymbol{\tau}_\mathbf{n} \cdot \mathbf{n})\mathbf{n},$$

where $\mathbf{n}$ is the outward normal to the wall surface, and $\boldsymbol{\sigma}_\mathbf{n}$ and $\boldsymbol{\tau}_\mathbf{n}$ are the normal components of the stress and extra-stress tensors, respectively.

Numerical method

The mathematical model described in the previous section was discretized in space with stabilized $P_1 - P_1$ finite elements [3]. The time discretization was performed with a backward difference formula (BDF) of order 3, and all simulations where performed with an

in house version of the freely available FEM software *LifeV* (see http://www.lifev.org/). This requires the differential problem (1) to be written in the weak form. Being Ω the fluid domain, let us define the Hilbert spaces $V = \boldsymbol{H}_0^1(\Omega)$ and $Q = L^2(\Omega)$. Formally multiplying equations (1) by suitable test functions and integrating by parts, yields

$$\begin{aligned} \int_\Omega \rho \left(\frac{\partial \mathbf{u}}{\partial t} + \mathbf{u} \cdot \nabla \mathbf{u} \right) \cdot \mathbf{v} + \int_\Omega \boldsymbol{\tau} : \nabla \mathbf{v} - \int_\Omega p \operatorname{div} \mathbf{v} = \int_\Gamma (\boldsymbol{\sigma} \cdot \boldsymbol{n}) \cdot \mathbf{v}, \quad \forall \mathbf{v} \in \mathbf{V} \\ \int_\Omega q \operatorname{div} \mathbf{v} = \mathbf{0}, \quad \forall \mathbf{q} \in \mathbf{Q}. \end{aligned} \tag{5}$$

The finite element method consists in substituting the functional spaces V and Q by suitable sequences of finite dimensional subspaces $\{V_h | h > 0\}$ and $\{Q_h | h > 0\}$ in which we can compute an approximate solution $(\mathbf{u}_h, p_h)$. A proper choice of these subspaces ensures that the problem is solvable in the finite dimensional spaces and the approximate solutions converge to the solution of (5) when $h \to 0$. The convective term is linearized in a semi-implicit way, by considering that at time step t^{k+1} we have $\mathbf{u}^{k+1} \cdot \nabla \mathbf{u}^{k+1} \approx \mathbf{u}^k \cdot \nabla \mathbf{u}^{k+1}$. Finally, in order to fully linearize the discrete problem, we use the approximation

$$\boldsymbol{\tau}^{k+1} = \mu(\dot{\gamma}^{k+1})(\nabla \mathbf{u}^{k+1} + (\nabla \mathbf{u}^{k+1})^T) \approx \mu(\dot{\gamma}^k)(\nabla \mathbf{u}^{k+1} + (\nabla \mathbf{u}^{k+1})^T).$$

The fully discrete problem then reads: Find $(\mathbf{u}_h, p_h) \in V_h \times Q_h$ such that

$$\begin{aligned} \int_\Omega \rho \left(\frac{11}{6\Delta t} {\mathbf{u}_h}^{k+1} + {\mathbf{u}_h}^k \cdot \nabla {\mathbf{u}_h}^{k+1} \right) \cdot \mathbf{v}_h + \int_\Omega \mu(\dot{\gamma}^k)(\nabla {\mathbf{u}_h}^{k+1} + (\nabla \mathbf{u}^{k+1})) : \nabla \mathbf{v}_h - \\ - \int_\Omega p_h \operatorname{div} \mathbf{v}_h = \int_\Omega \frac{1}{\Delta t} (3\mathbf{u}_h^k - \frac{3}{2}\mathbf{u}_h^{k-1} + \frac{1}{3}\mathbf{u}_h^{k-2}) \cdot \mathbf{v}_h + \\ + \int_\Gamma (\boldsymbol{\sigma} \cdot \boldsymbol{n}) \cdot \mathbf{v}_h, \qquad \forall \mathbf{v}_h \in V_h \end{aligned} \tag{6}$$

and

$$\int_\Omega q_h \operatorname{div} \mathbf{v}_h = 0, \qquad \forall q_h \in Q_h.$$

The computational effort necessary to perform the numerical simulation of the previous equations is of the same order of the Navier-Stokes equations. The extra computational load is related to the need, at each time step, of computing the shear rate. The BDF method can be memory consuming because the solutions in the previous three time steps need to be stored in memory.

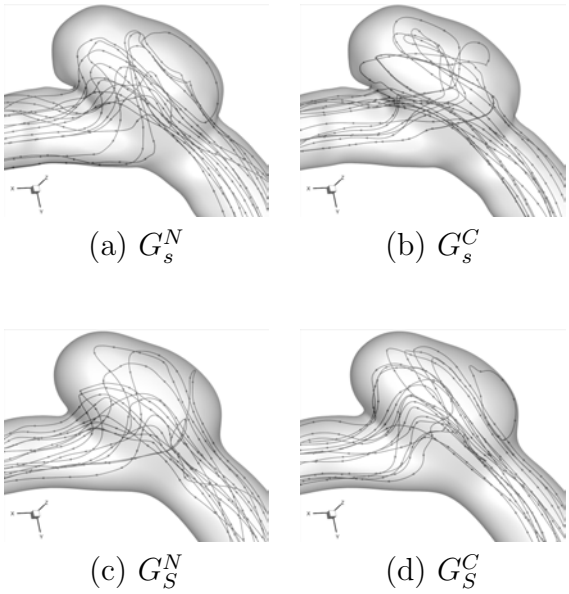

(a) G_s^N (b) G_s^C

(c) G_S^N (d) G_S^C

Figure 4: Particle tracking using identical seeding location at the aneurysm neck for the (a) Newtonian model on G_s (b) Carreau model on G_s (c) Newtonian model on G_S (d) Carreau model on G_S.

4 Numerical results and discussion

A total of four cases were studied with respect to uncertainty in both the geometry and constitutive model of the blood. In specific, geometries G_s and G_S, obtained from different smoothing intensities were considered, each with two different rheological models, Newtonian and Carreau. From here onwards the superscripts N and C will be used to refer to the Newtonian and Carreau models, respectively.

Numerical simulations were performed using graded meshes with element size of 0.16 mm within the aneurysm. This amounts to using around 0.85 M tetrahedral elements in each geometry.

Steady state solutions were sought however an instability associated to a small recirculation region at the distal portion of the aneurysm neck meant that this was in practice not achieved. The instability did not affect the flow upstream to this region, including within the aneurysm, while downstream a greater influence was noted. The simulations discussed here are taken at the same time step, at a total of 10 s after a steady inflow velocity was imposed, hence at time $T = t_{ramp} + 10$ s.

The general flow patterns within the aneurysm indicate separated flow in the overhang regions at the proximal and distal portions. Since the aneurysm is located on the outer bend of the artery, part of the core flow enters the aneurysm naturally, impacting the upper side wall and forming two counter rotating vortical structures. These spread out to fill the separated regions and later flow out of the aneurysm.

In Figure 4 the particle tracks for each case are depicted. These tracks are seeded

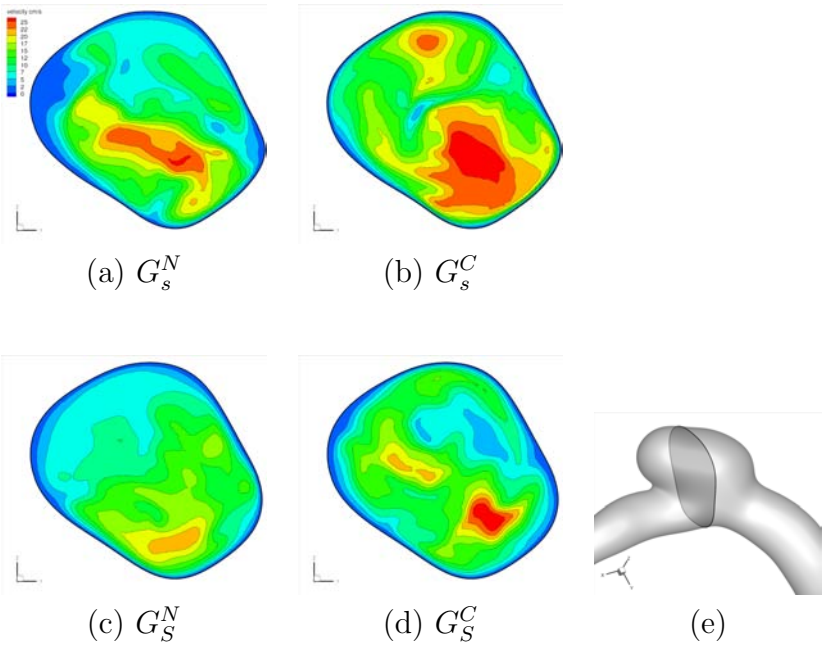

(a) G_s^N (b) G_s^C

(c) G_S^N (d) G_S^C (e)

Figure 5: Velocity magnitude in the slice cut (e). (a) Newtonian model on G_s (b) Carreau model on G_s (c) Newtonian model on G_S (d) Carreau model on G_S.

at the neck of the aneurysm, at the same locations for all cases. It is evident that both rheological model and geometry have a considerable impact on the resulting velocity field.

Moreover, from cross sections of the velocity magnitude shown in Figure 5 an emphatic difference in the flow field is perceived. We can also observe that for both solutions using G_s (hence G_s^C and G_s^N), the bulk of the velocity flux along the artery axis occurs in what the artery would have conceivably been. However, the aneurysm contains high velocity swirling motion that is driven from the neck of the aneurysm. For G_S a greater portion of flow with a higher velocity sweeps into the aneurysm, however this is seen to exit more readily and the regions of swirling and separated flow tend to be more contained.

Figure 6 displays the WSS distribution. Within the aneurysm the WSS is low, with values typically below 2 Pa and on average around 1.5 Pa. The highest values, around 8 Pa, are found at the distal portion of the neck. For this patient specific study, the geometry uncertainty given by the surface smoothing has an influence on the WSS comparable to that of different rheological models.

In order to quantify the differences in WSS given by these uncertainties, illustrated in Figure 7, the mean values are computed (for the aneurysm region shown only) and found to be $G_S^N - G_S^C = 0.63$ Pa, $G_s^N - G_s^C = 0.64$ Pa, $G_S^N - G_s^N = 0.61$ Pa, $G_S^C - G_s^C = 0.74$ Pa. While these values show that the geometrical and rheological uncertainty have a similar impact on the WSS, the peak differences are found to be more pronounced when comparing different models on the same geometry definition.

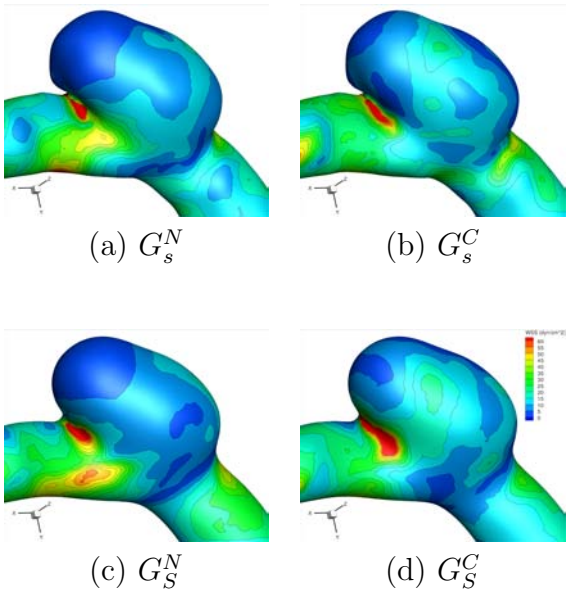

(a) G_s^N (b) G_s^C

(c) G_S^N (d) G_S^C

Figure 6: WSS for the (a) Newtonian model on G_s (b) Carreau model on G_s (c) Newtonian model on G_S (d) Carreau model on G_S. The scale is the same for all pictures.

Regarding the viscosity distribution obtained for the Carreau model, the average values of $\mu_S = 0.0337$ Poi and $\mu_s = 0.0334$ Poi were observed in G_S and G_s, respectively. It should be noted that these values are smaller than the constant Newtonian viscosity $\mu = 0.04$ Poi, chosen as an average high shear viscosity over the range $\dot{\gamma} \in [6, 1000]$ s $^{-1}$. In fact, the choice of the Newtonian viscosity, not addressed in this work fully, is yet another source of uncertainty. It was also observed that the higher viscosity values, near $\mu = 0.04$ Poi, are only found close to the inflow section, before the first bend, where the fluid starts exhibiting strong secondary flows.

5 CONCLUSIONS

The study presented is a preliminary work to study the effects of uncertainty on numerical simulations of cerebral aneurysms from *in vivo* medical data. The uncertainties were introduced in the form of variations in the geometry and fluid model, and significant differences were observed in solutions for both cases. This indicates that if under physiological conditions blood rheology includes non-Newtonian effects, these should not be neglected in the mathematical modeling. The presupposed argument that differences coming from the model choice are small, when compared to geometrical uncertainties, does not hold in the specific geometry presented here.

Naturally, the results obtained in this work are patient specific and do not necessarily extend to represent a general case. In order to be validated in a more general framework, a comprehensive study must be performed in a large representative patient database.

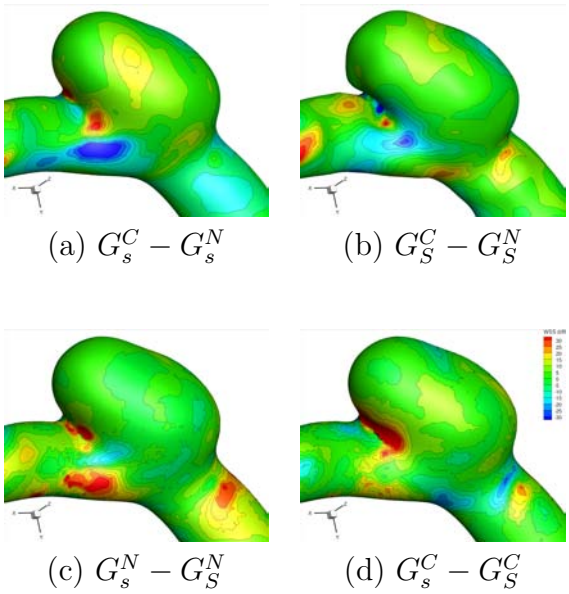

(a) $G_s^C - G_s^N$ (b) $G_S^C - G_S^N$

(c) $G_s^N - G_S^N$ (d) $G_s^C - G_S^C$

Figure 7: WSS difference between (a) the Carreau and the Newtonian models on G_s (b) the Carreau and the Newtonian models on G_S (c) the Newtonian model on G_s and G_S (d) the Carreau model on G_s and G_S.

Moreover, the analysis of a steady state solution is not physiological and the fully unsteady problem should be considered, using a realistic waveform. The prominent differences in computed flow field detected for steady flow are expected to be present in the time dependent simulations, however the extent cannot be inferred from these results.

Finally, it must be noted that uncertainty can come from other sources. These include: the use of different viscosity models based on distinct fitting procedures of the experimental data; the use of different structural models for the vessel wall and the inclusion of fluid-structure interaction; the inclusion of smaller side branches that are usually cut-off, inflow and outflow boundary conditions.

Acknowledgements

The authors acknowledge Prof. Jorge Campos and his team from FMUL (Portugal) for providing the rotational CTA medical image used in this study and Prof. Marina Kameneva from Univ. Pittsburgh (USA) for providing experimental viscosity data. This work has been partially supported by the Research Center CEMAT/IST through FCT's funding program and by the FCT project UTAustin/CA/0047/2008. The first and third authors are funded by FCT grants SFRH/BPD/44478/2008/ and SFRH/BPD/34273/2006, respectively.

REFERENCES

[1] M. Anand and K.R. Rajagopal, A shear-thinning viscoelastic fluid model for describing the flow of blood *Int. J. Cardiovascular Medicine and Science*, **4(2)**, 59–68 (2004).

[2] T. Bodnár and A. Sequeira, Numerical study of the significance of the non-Newtonian nature of blood in steady flow through a stenosed vessel. In: Advances in Mathematical Fluid Mechanics, A. Sequeira and R. Rannacher (eds), 83–104, *Springer Verlag* (2010).

[3] E. Burman and M. A. Fernández, Continuous interior penalty finite element method for the time-dependent Navier-Stokes equations: space discretization and convergence, *Numerische Mathematik*, **107**, Nr. 1, 39–77 (2007).

[4] A. M. Gambaruto, A. Moura and A. Sequeira, Topological flow structures and stir mixing for steady flow in a peripheral bypass graft with uncertainty, *International Journal for Numerical Methods in Biomedical Engineering* to appear.

[5] Y. I. Cho and K. R. Kensey, Effects of non-Newtonian viscosity of blood on flows in a diseased vessel. part I: steady flows, *Biorheology*, **28**, 241–262 (1991).

[6] L. Formaggia, A.M. Quarteroni and A. Veneziani (eds.), Cardiovascular Mathematics. Modeling and simulation of the circulatory system, Series: MS&A Vol.1, *Springer* (2009).

[7] J. Frosen *et al.*, Remodeling of saccular cerebral artery aneurysm wall is associated with rupture: Histological analysis of 24 unruptured and 42 ruptured cases, *Stroke*, **35**, 2287-2293 (2004).

[8] G.P. Galdi, R. Rannacher, A.M. Robertson and S. Turek, Hemodynamical Flows: Modeling, Analysis and Simulation, Series: Oberwolfach Seminars, *Birkhuser Verlag* (2008).

[9] G.J. Hademenos and T.F. Massoud, The Physics of Cerebrovascular Diseases: Biophysical Mechanisms of Development, Diagnosis and Therapy, Biological Physics Series, *Springer-Verlag* (1998).

[10] G. D. O. Lowe (ed.), Clinical blood rheology, *CRC Press, Boca Raton, FL* (1988).

[11] S. O. Oktar *et al.*, Blood-flow volume quantification in internal carotid and vertebral arteries: comparison of 3 different ultrasound techniques with phase-contrast MR imaging, *American Journal of Neuroradiology*, **27**, 363–369 (2006).

[12] M.A. Robertson, A. Sequeira and M. Kameneva, Hemorheology. In: Hemodynamical Flows: Modeling, Analysis and Simulation, Oberwolfach Seminars, *Birkhuser*, **37**, 63-120 (2008).

[13] M.A. Robertson, A. Sequeira and R. Owens, Rheological models for blood. In: Cardiovascular Mathematics. Modeling and simulation of the circulatory system. L. Formaggia, A.M. Quarteroni and A. Veneziani (eds), Series: MS&A *Springer*, **Vol.1**, 213–244 (2009).